

On the GJ 436 planetary system

G. Maciejewski¹, A. Niedzielski¹, G. Nowak^{2,3}, E. Pallé^{2,3},
B. Tingley^{2,3,4}, R. Errmann^{5,6}, and R. Neuhauser⁵

¹Centre for Astronomy, Faculty of Physics, Astronomy and Informatics, Nicolaus Copernicus University, Grudziadzka 5, 87-100 Torun, Poland
e-mail: gm@astri.umk.pl

²Instituto de Astrofísica de Canarias, C/ vía Láctea, s/n, E-38205 La Laguna, Tenerife, Spain

³Departamento de Astrofísica, Universidad de La Laguna, Av. Astrofísico Francisco Sánchez, s/n, E-38206 La Laguna, Tenerife, Spain

⁴Stellar Astrophysics Centre, Institut for Fysik og Astronomi, Aarhus Universitet, Ny Munkegade 120, 8000 Aarhus C, Denmark

⁵Astrophysikalisches Institut und Universitäts-Sternwarte, Schillergässchen 2–3, 07745 Jena, Germany

⁶Institute of Applied Physics, Abbe Center of Photonics, Friedrich-Schiller-Universität Jena, Max-Wien-Platz 1, 07743 Jena, Germany

Received —, 2014

ABSTRACT

The GJ 436 system contains a transiting planet GJ 436 b which is a hot analogue of Neptune on an eccentric orbit. Recently, two additional transiting sub-Earth planets have been postulated in the literature. We observed three transits of GJ 436 b over the course of 3 years using two-meter class telescopes, each with a photometric precision better than one millimagnitude. We studied system dynamics based on the existence of the additional planets. We redetermined system parameters, which were in agreement with those found in the literature. We refined the orbital period of GJ 436 b and found no evidence of transit timing variations. The orbital motion of the GJ 436 c planet candidate was found to be significantly affected by the planet b with variations in transit times at a level of 20 minutes. As the orbital period of the GJ 436 d planet candidate remains unknown, our numerical experiments rule out orbits in low-order resonances with GJ 436 b. The GJ 436 system with the hot Neptune and additional two Earth-like planets, if confirmed, would be an important laboratory for studies of formation and evolution of planetary systems.

Key words: *planetary systems – stars: individual: GJ 436 – planets and satellites: individual: GJ 436 b, GJ 436 c, GJ 436 d*

1. Introduction

The GJ 436 planetary system, with one confirmed planet and two proposed planets, may be the first multiple-transiting-planet system initially discovered from the ground. The host star – an M3 dwarf with an age of several Gyr, located 10 pc from the Sun – was found to have a Neptune-mass planetary companion on a 2.64 day orbit with the precise radial velocity (RV) technique (Butler *et al.* 2004). Additional Doppler measurements found an orbit that was far from circular, with

an eccentricity of $e_b = 0.16 \pm 0.02$ (Maness *et al.* 2007) and the semi-major axis of which is $a_b = 0.0285$ AU. Gillon *et al.* (2007b) later detected planetary transits in photometry of the host star. Combining the spectroscopic and photometric data allowed those authors to determine the planet's mass of $M_b = 22.6 \pm 1.9 M_\oplus$ (Earth masses) and radius of $R_b = 25200 \pm 2200$ km = $3.95 \pm 0.34 R_\oplus$ (Earth radii). These properties showed that GJ 436 b must be a planet similar to Uranus or Neptune, but much closer to its host star. Due to this proximity, the planet's atmosphere is hot, with an equilibrium temperature between 520 and 620 K. These features offer unique opportunities for a number of follow-up observations conducted with ground-based and space-born facilities.

Maness *et al.* (2007) and Deming *et al.* (2007) have postulated that the non-zero eccentricity could be caused by an unseen planetary companion. Based on available RV data, Ribas *et al.* (2008a) found a sign of additional planet close to the 2:1 mean motion resonance with GJ 436 b. Coughlin *et al.* (2008) indicated that orbital inclination, transit depth, and transit duration may exhibit variations excited by gravitational influence of another planet in a non-resonant orbit. On the other hand, dynamical studies of Alonso *et al.* (2008) and Bean & Seifahrt (2008) eliminated the proposed 2:1 configuration, and placed physical limitations on possible configurations of the second planet in the system.

Using the Spitzer Space Telescope, Stevenson *et al.* (2012) detected additional shallow transit-like features in the light curve of GJ 436. They propose that these features could be caused by transits of two additional planets with radii of $\approx 0.7 R_\oplus$. The orbital period of the planet candidate GJ 436 c (originally labelled UCF-1.01) was found to be 1.37 d, while the orbital period of GJ 436 d (UCF-1.02) could not be determined because only two transits were observed. Assuming a range of bulk densities typical for terrestrial planets (*i.e.*, between 3 and 8 g cm⁻³), the masses of both planet candidates were constrained to 0.15–0.40 M_\oplus – much below a detection threshold of current most advanced RV surveys. The orbital period ratio of GJ 436 b and GJ 436 c is 1.94, close to a 2:1 orbital resonance which is generally thought to produce strong transit time variations (TTVs). Recent studies by Lanotte *et al.* (2014) and Stevenson *et al.* (2014) show that the existence of both planet candidates still remains disputable.

It is believed that future space-based instruments will provide opportunities to confirm the multi-planetary architecture of the GJ 436 system. We note, however, that TTV observations from the ground and dynamical studies may place some constraints on possible planetary configurations. In this paper, we explore the possibility of the proposed multi-planetary architecture, using new upper limits on the TTVs of GJ 436 b based on our photometric observations and combining this with a dynamical model of the system.

2. Observations and data reduction

We observed the 2011 Jan 04 transit of GJ 436 b with the 2.2-m telescope at the Calar Alto Observatory (Spain) as a back-up target within the program F11-2.2-008, which was focused on transit timing of the WASP-12 b planet. The Calar Alto Faint Object Spectrograph (CAFOS) in imaging mode was used to acquire the light curve in the Cousin R filter. To shorten the read-out time, the original field of view (FoV) was windowed to $5.3' \times 6.5'$. Observations were occasionally affected by passing thin clouds. We observed a second transit on 2012 Feb 02 with the Nordic Optical Telescope (NOT) at the Observatorio del Roque de los Muchachos, La Palma (Spain), as a backup target of the P44-102 observing program (OPTICON 2011B/003), the goal of which was acquiring high-precision transit light curves for WASP-12 b's transits. The Andalucia Faint Object Spectrograph and Camera (ALFOSC) was used in an imaging mode, windowed to the $6.4' \times 6.4'$ FoV. Photometric time series was taken in the Bessel R filter under excellent weather conditions.

Both instruments used 2×2 binning for faster readout. Autoguiding guaranteed that stellar centroids did not change their locations on the detector matrix during each run. We defocused the telescopes significantly, creating doughnut-like stellar profiles and spreading the light over many pixels, which enabled longer exposure times and reduced the impact of flat-fielding imperfections. This also improves duty cycle, as the ratio of time during exposure versus read-out is improved, allowing more photons to be gathered during transit and thereby increasing the photometric efficiency. We reduced the observations with standard procedures, including de-biasing and flat-fielding using sky flats. We performed differential aperture photometry with respect to nearby comparison stars BD+27 2046 and TYC 1984-1884-1. Radii of the aperture and background ring were empirically optimized to produce the smallest scatter in the out-of-transit light curve.

We obtained an additional transit light curve from observations made on 2014 Mar 23 from low-resolution spectra acquired with the NOT/ALFOSC. For these observations we chose the 2×2 binning mode, a readout speed of 200 pixel/sec with a gain of $0.327 \text{ e}^-/\text{ADU}$ and a readout noise of $4.2 \text{ e}^-/\text{pixel}$. We used ALFOSC in its long-slit spectroscopic mode, selecting the grism #4 which covers the spectral range $3200 - 9100 \text{ \AA}$ and a custom-built slit of a width of 40 arcsec. We chose BD+27 2046 as reference, which has similar brightness and is located at a distance of 3.81 arcmin from GJ 436. The position angle of the reference star with respect to the target was equal to 37.39° . Observations began at 01:31 UT (35 minutes before ingress) and ended at 03:18 UT (10 minutes after egress). The exposure time was set to 60 seconds and the readout time of instrument was 9 s, meaning we collected approximately one spectrum every 69 s. The data reduction (bias and flat-field corrections, extraction of the spectra and corresponding calibration arcs as well as wavelength calibration using the He and Ne lamps) was made using an

IRAF¹ script written for NOT/ALFOSC long-slit data. Optimal extraction of the spectra was obtained using an aperture width of ± 10 binned pixels, which corresponds to 7.6 arcsec on the detector. This is 2 to 5.5 times the raw seeing during the observations (1.4 – 3.7 arcsec). The light curve was constructed using 1/3 of spectra of the target and reference star centered at the maximum of the GJ 436 spectrum. The maximum of the spectral energy distribution was found at 790 nm that corresponds to the central passband of the photometric I filter.

Differential atmospheric extinction and differences in spectral types of the target and comparison stars, as well as instrumental effects caused by the field derotator in NOT data, are expected to produce photometric trends, whose time scale is similar to the duration of the run. The de-trending procedure was done with the JKTEBOP code (Southworth *et al.* 2004a,b) by fitting a second-order polynomial function of time along with a trial transit model and then subtracting the resulting polynomial from the light curve. Magnitudes were transformed into fluxes, which were normalized to unity outside of the transit. The timestamps in geocentric Julian dates in coordinated universal time (UTC) were provided by a GPS system and verified with the network time protocol software, then converted to barycentric Julian dates in barycentric dynamical time (BJD_{TDB}, Eastman *et al.* 2010). The observing details and data quality characteristics are given in Table 1.

Table 1

New transit light curves reported for GJ 436 b: date UT is given for the middle of the transit, X shows a course of changes in airmass during transit observations, t_{exp} is the exposure time, Γ is the median number of exposures per minute, pnr is the photometric scatter in millimagnitudes per minute of observation, as defined by Fulton *et al.* (2011).

| # | Date UT | Telescope | X | t_{exp} (s) | Γ | pnr (mmag) |
|---|-------------|------------------|--------------------|---------------|----------|--------------|
| 1 | 2011 Jan 04 | 2.2-m Calar Alto | 1.08 → 1.02 → 1.07 | 12 | 1.76 | 0.6 |
| 2 | 2012 Feb 02 | 2.6-m NOT | 1.08 → 1.00 → 1.06 | 20 | 2.07 | 0.3 |
| 3 | 2014 Mar 23 | 2.6-m NOT | 1.01 → 1.18 | 60 | 0.87 | 0.7 |

3. Results

We used different codes to model the transit light curves and analyze the RV and timing datasets. We obtained the final results of this study by iterating the different codes until we reached convergence. Sections 3.1 and 3.2 contain a description of the steps involved in each iteration.

¹IRAF is distributed by the National Optical Astronomy Observatory, which is operated by the Association of Universities for Research in Astronomy (AURA) under cooperative agreement with the National Science Foundation.

3.1. Transit light curves

We modeled the new sub-millimagnitude precision light curves simultaneously with the Transit Analysis Package² (TAP, Gazak *et al.* 2012). This code employs the Markov Chain Monte Carlo (MCMC) method, including the Metropolis-Hastings algorithm and a Gibbs sampler, to find the best-fit parameters of a transit light curve approximated by the analytical model of Mandel & Agol (2002). The time-correlated noise in data (so called red noise) is investigated with the Carter & Winn (2009) wavelet parametrization. This approach is known to provide conservative uncertainty estimates. TAP parametrizes the flux distribution across the stellar disk with a quadratic limb darkening (LD) law (Kopal 1950). The values of linear and quadratic LD coefficients, u_1 and u_2 respectively, were linearly interpolated from tables of Claret & Bloemen (2011) with an on-line tool³ of the EXOFAST package (Eastman *et al.* 2013). The stellar parameters for GJ 436 were taken from von Braun *et al.* (2012), assuming solar metallicity.

The fitting procedure kept the orbital inclination i_b , the semimajor-axis scaled by stellar radius a_b/R_* , and the planetary to stellar radii ratio R_b/R_* as free parameters, linked together for all light curves. The mid-transit times were determined independently for each light curve. The orbital period was fixed at a value from a refined ephemeris. The LD coefficients were allowed to vary around the theoretical values under the Gaussian penalty of $\sigma = 0.05$, independently for all three datasets. This allowed us to account not only for differences between R and I bands, but also for any possible differences in instrumental implementation of R -band filters. The orbital eccentricity e_b and longitude of periastron ω_b were taken from the dynamical model discussed in Sect. 3.2. The new light curves with the best-fit transit model are plotted in Fig. 1.

Our new transit observations prolong the timespan covered by observations and allow the transit ephemeris to be refined. The derived mid-transit times were combined with the literature ones to calculate new reference epoch T_0 and orbital period P_b .

The parameters of our best-fit model are given in Table 2, together with recent literature results for comparison. We also list the resulting system properties: the transit parameter b_b , defined as

$$b_b = \frac{a_b}{R_*} \frac{1 - e_b^2}{1 + e_b \cos \omega_b} \cos i_b, \quad (1)$$

and the mean stellar density ρ_* , which can be directly calculated from transit observable properties with a formula derived from Kepler's third law

$$\rho_* = \frac{3\pi}{GP_b^2} \left(\frac{a_b}{R_*} \right)^3, \quad (2)$$

²<http://ifa.hawaii.edu/users/zgazak/IfA/TAP.html>

³<http://astroutils.astronomy.ohio-state.edu/exofast/limbdark.shtml>

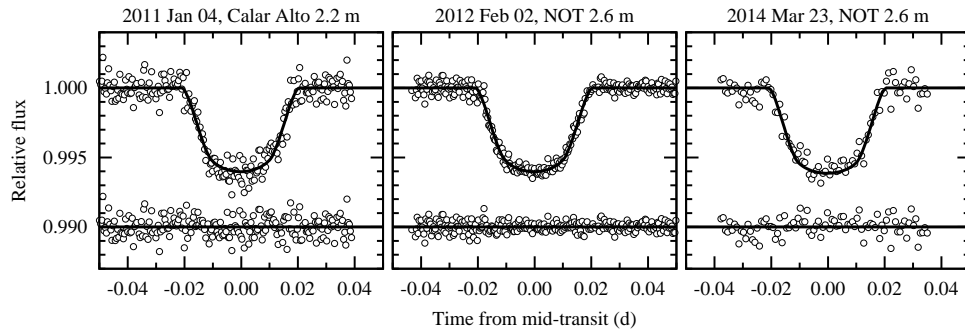


Fig. 1. New transit light curves for GJ 436 b with the best-fit model, plotted with solid lines. The residuals are shown in bottom parts of the panels.

where G is the gravitational constant.

Table 2

Parameters of the GJ 436 system derived from modeling transit light curves.

| Parameter | This work | von Braun <i>et al.</i> (2012) | Lanotte <i>et al.</i> (2014) |
|-----------------------------|------------------------------|--|--|
| i_b ($^\circ$) | $86.44^{+0.17}_{-0.16}$ | $86.6^{+0.1}_{-0.1}$ | $86.858^{+0.049}_{-0.052}$ |
| a_b/R_* | $13.73^{+0.46}_{-0.43}$ | – | $14.54^{+0.14}_{-0.15}$ |
| R_b/R_* | $0.0822^{+0.0010}_{-0.0011}$ | 0.0833 ± 0.0002 | – |
| b_b | $0.736^{+0.042}_{-0.041}$ | $0.853^{+0.003}_{-0.003}$ | $0.7972^{+0.0053}_{-0.0055}$ |
| ρ_* (ρ_\odot) | $4.97^{+0.50}_{-0.47}$ | $5.37^{+0.30}_{-0.27}$ | $5.91^{+0.17}_{-0.18}$ |
| T_0 (BJD _{TDB}) | $2454510.80162 \pm 0.00007$ | $2454510.80096 \pm 0.00005$ | – |
| P_b (d) | $2.64389754 \pm 0.00000043$ | $2.64389826^{+0.00000056}_{-0.00000058}$ | $2.64389803^{+0.00000027}_{-0.00000025}$ |

3.2. Dynamical model with the GJ 436 c planet candidate

The linear fit to mid-transit times for GJ 436 b results in a reduced χ^2 equal to 5.5, which indicates a marked departure from a linear ephemeris (Stevenson *et al.* 2012). The periodogram analysis reveals no statistically significant periodic signal, so stellar activity, systematic effects, or underestimated timing errors may be a source of a spurious timing variations. An upper limit on the amplitude of any periodic signal in transit timing was found to be 0.0002 d.

Mid-transit times for the GJ 436 c planet candidate show noticeable departure from a linear ephemeris (Stevenson *et al.* 2012) that suggests planet’s orbital motion is perturbed by the planet b. To study the mutual interactions between both planets, a two-planet dynamical model was constructed with the Systemic code in version 2.16 (Meschiari *et al.* 2009). We used 113 RV measurements from Knutson *et al.* (2014), acquired with the HIRES echelle spectrometer at the Keck I telescope between January 2000 and December 2010. We also used 171 HARPS RVs obtained

between January 2009 and April 2010 from Lanotte *et al.* (2014). For GJ 436 b, we used mid-transit times for 37 epochs available in the literature (Gillon *et al.* 2007a,b; Shporer *et al.* 2009; Cáceres *et al.* 2009; Deming *et al.* 2007; Alonso *et al.* 2008; Knutson *et al.* 2011; Pont *et al.* 2009; Bean *et al.* 2008; Ribas *et al.* 2008b; Coughlin *et al.* 2008; Ballard *et al.* 2010; Beaulieu *et al.* 2011) and 3 new determinations reported in this paper. In addition, we used 15 mid-occultation times from Stevenson *et al.* (2010) and Knutson *et al.* (2011). The best-fit Newtonian solution was found with a differential evolution algorithm using 5000 steps, followed by a number of iterations of Levenberg-Marquardt optimization. The Runge-Kutta-Fehlberg (RK45) algorithm was used to integrate equations of motion with an accuracy requirement of 10^{-16} . The bootstrap method with 10^3 trials was used to estimate parameter uncertainties, calculated as median absolute deviations. The orbital periods, eccentricities, and arguments of periapsis were left free for both planets. The mass of the planet candidate was fixed at the value of $0.28 M_{\oplus}$ (Earth masses) taken from Stevenson *et al.* (2012). The mass of planet b was allowed to vary. Orbital inclinations were taken from our transit light-curve analysis (Sect. 3.1) for GJ 436 b and from Stevenson *et al.* (2012) for the planet candidate. The parameters of the best-fit dynamical model are listed in Table 3.

Table 3

Orbital parameters for the GJ 436 b planet and GJ 436 c planet candidate from the two-planet dynamical model. The values are given for the epoch JD 2455959.

| Parameter | GJ 436 b | GJ 436 c |
|-------------------------------|-----------------------------|---------------------------------|
| Orbital period (d) | $2.64388312 \pm 0.00000057$ | 1.365960 ± 0.000012 |
| Semi-major axis (AU) | 0.0291 ± 0.0015 | $0.01871^{+0.00097}_{-0.00094}$ |
| Orbital eccentricity | 0.13827 ± 0.00018 | 0.1166 ± 0.0046 |
| Longitude of periastron (deg) | 351.00 ± 0.03 | 36.50 ± 0.41 |
| RV amplitude (m/s) | 17.09 ± 0.22 | 0.3* |
| Mass (M_{\oplus}) | 22.1 ± 2.3 | 0.28** |

* predicted value

** value taken from Stevenson *et al.* (2012).

The SWIFT’s Regularized Mixed Variable Symplectic (RMVS) integrator was used to trace the evolution of orbital parameters, which exhibit oscillatory patterns as a function of time. The best-fit dynamical model is stable in a timescale of 10^6 yr (over 130 million orbits of GJ 436 b) and yields strong constraints on the eccentricity of the GJ 436 c planet candidate. Its best-fit value is similar to that one for GJ 436 b but it is expected to oscillate between a value as small as 0.02 and 0.19 with a period of 35.4 yr (Fig. 2a), at anti-phase with marginal variations in e_b (between 0.137 and 0.139; the range is smaller by a factor of the mass ratio that is a consequence of conservation of momentum). The predicted variation in orbital

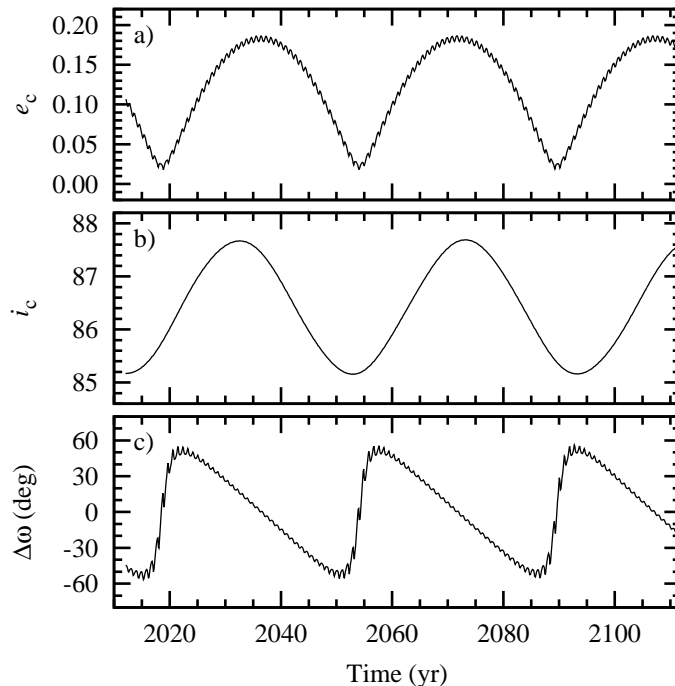


Fig. 2. Evolution of the orbital eccentricity and inclination for the GJ 436 c planet candidate (panels a and b) and difference in arguments of periastris between GJ 436 b and c.

inclination for GJ 436 c is 2.6° (Fig. 2b). The inclination of GJ 436 b's orbit was found to decrease with a rate of 0.025 degree per century – far under the detection threshold of current transit observations. The ratio between the orbital periods of both planets, $P_b/P_c = 1.94$, suggests the planets are close to a 2:1 commensurability and could be trapped in a mean motion resonance. The evolution of the difference between arguments of periastron, defined as $\Delta\omega = \omega_b - \omega_c$, is plotted in Fig. 2c. The periastrons were found to be in apsidal alignment around 0° and librate with an amplitude of 56° . Such conditions are generated by the linear secular coupling and prevent both planets from close encounters which could destabilize the system. The eccentricity-type resonant angles, defined as a linear combination of mean longitudes λ and arguments of periastron,

$$\theta_b = \lambda_c - 2\lambda_b + \omega_b \quad (3)$$

$$\theta_c = \lambda_c - 2\lambda_b + \omega_c \quad (4)$$

show no libration, so both planets are not in a dynamical resonance.

Figure 3 shows transit timing residuals for GJ 436 b and the GJ 436 c planet candidate, produced by mutual gravitational interactions. For both planets, the signal is periodic with a period of 41.2 d. The range of variation is substantial for the GJ 436 c planet candidate with a value of almost 20 min. Timing of GJ 436 b is predicted to be modulated with an amplitude of 16 s – a signal which is under the

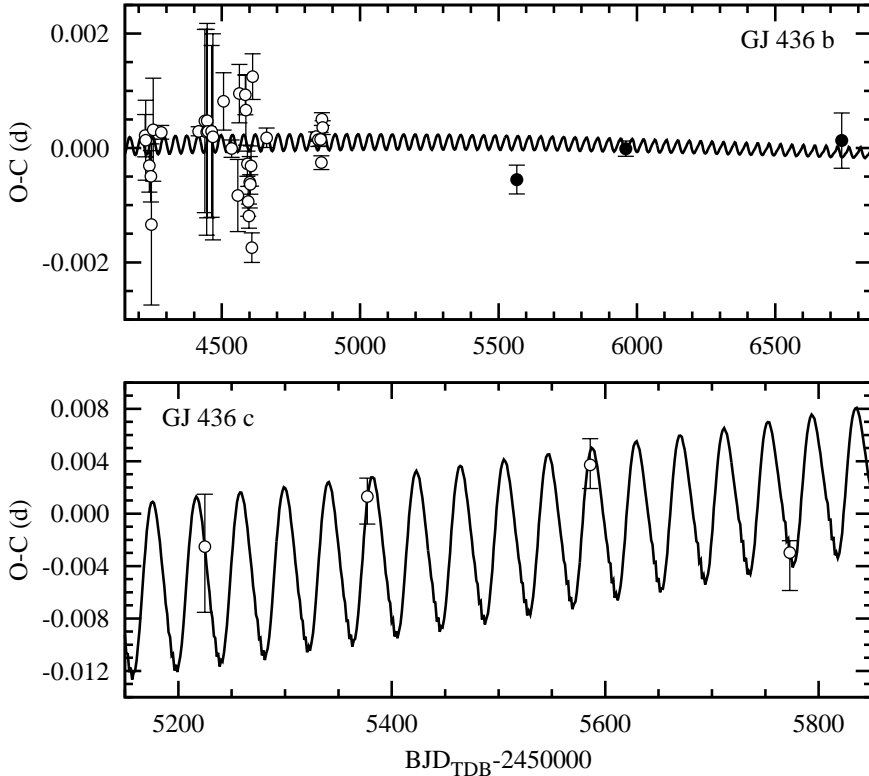


Fig. 3. Timing residuals for transits of the GJ 436 b planet and the GJ 436 c planet candidate, resulting from mutual gravitational interactions.

detection threshold of the current timing dataset.

3.3. Constraints on the orbital period of the GJ 436 d planet candidate

The period of time between the two observations of the transits of candidate GJ 436 d, $\tau_d = 151.5$ d, must be a multiple of a true orbital period P_d . Stevenson *et al.* (2012) estimate the upper limit for P_d to be 5.56 d, based on 1- σ uncertainty in transit duration of the planet candidate. We note however, that the fact that the orbital inclination is unknown weakens their argument. Periods shorter than P_b may be excluded because no transit signature was found in the 2.4-day long continuous light curve of GJ 436 acquired with the Spitzer Space Telescope at 8 μm (Stevenson *et al.* 2012). We used GJ 436 b's transit timing and system's dynamical stability to put constraints on P_d .

Using the Systemic code, we conducted a numerical experiment in which the planet d was inserted into the two-planet system derived in Sect. 3.2. The mass of the planet d was set to $0.27 M_{\oplus}$ as given by Stevenson *et al.* (2012). The orbital eccentricity, e_d , varied between 0.0 and 0.3 with a step of 0.05. The initial value of the argument of periastron was set equal to ω_b and initial orbital longitude was

shifted by 180° with respect to the value for GJ 436 b at the epoch 0. The orbital inclination of the planet d was the same as for GJ 436 b. The value of P_d satisfied the relation

$$\tau_d = n \cdot P_d, \quad (5)$$

where n is 1, 2, 3... Each configuration was integrated with the RK45 algorithm, covering 2500 days, *i.e.*, the time span of the transit observations for GJ 436 b. The times of mid-transit times were extracted and the amplitude of periodic deviations from a linear ephemeris was calculated. In addition, each configuration was checked for the dynamical stability in 10^3 yr with the SWIFT's RMVS integrator. Configurations which were found to be unstable, mainly with $P_d < 3/2P_b$, were skipped.

The exemplary results for e_d equal to 0.05, 0.15, and 0.25 are shown in Fig. 4. Configurations with P_d/P_b close to 3:2 and 2:1 resonances would generate TTV signals above a detection threshold even for low-eccentricity orbits of the planet d. For greater eccentricities, configurations with resonances close to 3:1 or 5:2 would produce detectable TTVs.

4. Concluding discussion

Our new observations of GJ 436 b's transits allowed us to refine transit ephemeris and to redetermine system parameters. They prolong the timespan covered by observations by a factor of 3. They were combined with photometric and Doppler data from the literature in order to study dynamics of the system with two low-mass planet candidates.

The interferometric measurements for the GJ 436 host star give a precise value of stellar radius of $R_* = 0.455 \pm 0.018 R_\odot$ (von Braun *et al.* 2012), and when combined with a mean stellar density of $\rho_* = 4.97^{+0.50}_{-0.47} \rho_\odot$ results in a stellar mass of $M_* = 0.47 \pm 0.07 M_\odot$. This value is between $0.452^{+0.014}_{-0.012} M_\odot$ and $0.507^{+0.071}_{-0.062} M_\odot$ reported by Torres (2007) and von Braun *et al.* (2012), respectively. It is also still consistent within a $1-\sigma$ range with the value of $0.556^{+0.071}_{-0.065} M_\odot$ given by Lanotte *et al.* (2014). The deduced stellar surface gravity is $\log g_* = 4.792^{+0.047}_{-0.044}$ in cgs units, consistent with $\log g_* = 4.83 \pm 0.03$ derived by von Braun *et al.* (2012). Our determinations of the GJ 436 b's radius $R_b = 0.372 \pm 0.015 R_{Jup}$ and mean density $\rho_b = 1.35 \pm 0.22 \rho_{Jup}$ agree with the recent literature values within $1-\sigma$ ($0.369 \pm 0.015 R_{Jup}$ and $1.55^{+0.12}_{-0.10} \rho_{Jup}$ reported by von Braun *et al.* 2012, and $0.366 \pm 0.014 R_{Jup}$ and $1.6 \rho_{Jup}$ given by Lanotte *et al.* 2014). Our value of planetary mass $M_b = 22.1 \pm 2.3 M_\oplus$ is in a perfect agreement with $M_b = 22.6 \pm 1.9 M_\oplus$ given by Gillon *et al.* (2007b), but seems to be slightly underestimated comparing to $24.8^{+2.2}_{-2.5} M_\oplus$ of von Braun *et al.* (2012) and $25.4^{+2.1}_{-2.0} M_\oplus$ of Lanotte *et al.* (2014). This is a direct consequence of higher stellar mass determined in both studies.

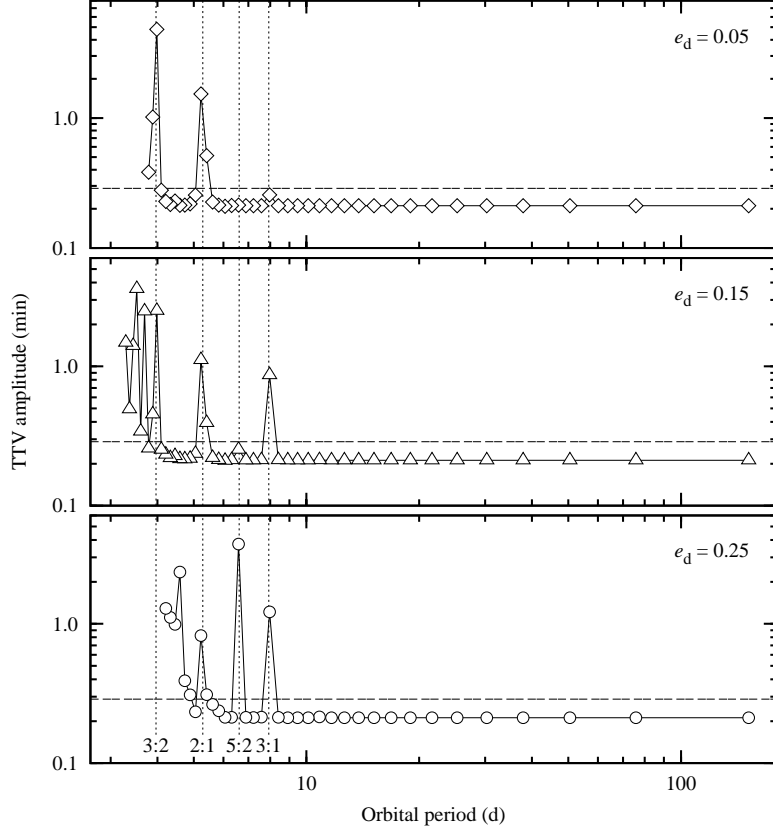


Fig. 4. Amplitude of a hypothetical TTV signal for GJ 436 b induced by the GJ 436 d planet candidate as a function of possible values of P_d for selected values of e_d . Only configurations that are stable for a time scale of 10^3 yr are shown. The horizontal dashed lines show a detection threshold based on observations. Vertical dotted lines mark selected P_d to P_b resonances.

Mid-transit times reported in this study follow a linear ephemeris with residuals smaller than 2σ . The transit from 2011 Jan 04 (JD 2455565.7), the most outlying from the linear ephemeris in our sample, could be affected by stellar activity at the ingress phase because photometric residuals from the transit model seem to exhibit some distortion. The lack of a periodic or semi-periodic TTV signal indicates that GJ 436 b is not noticeably perturbed by gravitational interactions with other bodies in the system. On the other hand, the orbital motion of the GJ 436 c planet candidate is significantly influenced by GJ 436 b. Our numerical model predicts that periastrons of both planets are in apsidal alignment. The TTV signal for GJ 436 c is expected to be at the level of 20 min and constrains the orbital eccentricity of the planet. Further precise transit observations for GJ 436 c will shed new light for system dynamics.

The orbital period of the GJ 436 d planet candidate remains unknown but the lack of the TTV signal for GJ 436 b put some constraints on it. Configurations

in which both bodies are close to low-order resonances are unlikely because they would generate detectable TTVs for GJ 436 b. A system with planets out of resonance is in line with statistical studies based on data from the space-based *Kepler* transit survey, which show that configurations with planets in close proximity to a resonance are not favoured (Fabrycky *et al.* 2014).

Acknowledgements. We would like to thank NOT and Calar Alto staff for their help during observing runs. GM acknowledges the financial support from the Polish Ministry of Science and Higher Education through the Iuventus Plus grant IP2011 031971. GM and AN acknowledge funding from the European Community's Seventh Framework Programme (FP7/2007-2013) under grant agreement number RG226604 (OPTICON). AN is supported by the Polish Ministry of Science and Higher Education grant N N203 510938. We would like to thank the German national science foundation Deutsche Forschungsgemeinschaft (DFG) for financial support for the Calar Alto run in program NE 515 / 44-1. RE would like to thank DFG for support in the Priority Programme SPP 1385 in project NE 515 / 34-1 and the Abbe School of photonics for the grant. The research is based on data collected with the Nordic Optical Telescope, operated on the island of La Palma jointly by Denmark, Finland, Iceland, Norway, and Sweden, in the Spanish Observatorio del Roque de los Muchachos of the Instituto de Astrofísica de Canarias. Some observations were made at the Centro Astronómico Hispano Alemán (CAHA), operated jointly by the Max-Planck Institut für Astronomie and the Instituto de Astrofísica de Andalucía (CSIC). Data presented here were obtained with ALFOSC, which is provided by the Instituto de Astrofísica de Andalucía (IAA) under a joint agreement with the University of Copenhagen and NOTSA.

REFERENCES

- Alonso, R., Barbieri, M., Rabus, M., *et al.* 2008, *A&A*, **487**, L5.
 Ballard, S., Christiansen, J. L., Charbonneau, D., *et al.* 2010, *ApJ*, **716**, 1047.
 Bean, J. L., Benedict, G. F., Charbonneau, D., *et al.* 2008, *A&A*, **486**, 1039.
 Bean, J. L., & Seifahrt, A. 2008, *A&A*, **487**, L25.
 Beaulieu, J.-P., Tinetti, G., Kipping, D. M., *et al.* 2011, *ApJ*, **731**, 16.
 Butler, R. P., Vogt, S. S., Marcy, G. W., *et al.* 2004, *ApJ*, **617**, 580.
 Cáceres, C., Ivanov, V. D., Minniti, D., *et al.* 2009, *A&A*, **507**, 481.
 Carter, J. A., & Winn, J. N. 2009, *ApJ*, **704**, 51.
 Claret, A., & Bloemen, S. 2011, *A&A*, **529**, A75.
 Coughlin, J. L., Stringfellow, G. S., Becker, A. C., *et al.* 2008, *ApJ*, **689**, L149.
 Deming, D., Harrington, J., Laughlin, G., *et al.* 2007, *ApJ*, **667**, L199.
 Eastman, J., Siverd, R., and Gaudi, B. S. 2010, *PASP*, **122**, 935.
 Eastman, J., Gaudi, B. S., & Agol, E. 2013, *PASP*, **125**, 83.
 Fabrycky, D. C., Lissauer, J. J., Ragozzine, D., *et al.* 2014, *ApJ*, **790**, 146.
 Fulton, B. J., Shporer, A., Winn, J. N., *et al.* 2011, *AJ*, **142**, 84.
 Gazak, J. Z., Johnson, J. A., Tonry, J., *et al.* 2012, *Advances in Astronomy*, **2012**, 697967.
 Gillon, M., Demory, B.-O., Barman, T., *et al.* 2007a, *A&A*, **471**, L51.
 Gillon, M., Pont, F., Demory, B.-O., *et al.* 2007b, *A&A*, **472**, L13.

- Knutson, H. A., Madhusudhan, N., Cowan, N. B., *et al.* 2011, *ApJ*, **735**, 27.
- Knutson, H. A., Fulton, B. J., Montet, B. T., *et al.* 2014, *ApJ*, **785**, 126.
- Kopal, Z. 1950, *Harvard Col. Obs. Circ.*, **454**, 1.
- Lanotte, A. A., Gillon, M., Demory, B.-O., *et al.* 2014, *A&A*, **572**, A73.
- Mandel, K., & Agol, E. 2002, *ApJL*, **580**, L171.
- Maness, H. L., Marcy, G. W., Ford, E. B., *et al.* 2007, *PASP*, **119**, 90.
- Meschiari, S., Wolf, A. S., Rivera, E., *et al.* 2009, *PASP*, **121**, 1016.
- Pont, F., Gilliland, R. L., Knutson, H., *et al.* 2009, *MNRAS*, **393**, L6.
- Ribas, I., Font-Ribera, A., & Beaulieu, J.-P. 2008a, *ApJ*, **677**, L59.
- Ribas, I., Font-Ribera, A., Beaulieu, J.-P., *et al.* 2008b, *Proceedings IAU Symposium*, **253**, 149.
- Shporer, A., Mazeh, T., Pont, F., *et al.* 2009, *ApJ*, **694**, 1559.
- Southworth, J., Maxted, P. F. L., & Smalley, B. 2004a, *MNRAS*, **349**, 547.
- Southworth, J., Maxted, P. F. L., & Smalley, B. 2004b, *MNRAS*, **351**, 1277.
- Stevenson, K. B., Harrington, J., Nymeyer, S., *et al.* 2010, *Nature*, **464**, 1161.
- Stevenson, K. B., Harrington, J., Lust, N. B., *et al.* 2012, *ApJ*, **755**, 9.
- Stevenson, K. B., Bean, J. L., Fabrycky, D., & Kreidberg L. 2014, *ApJ*, **796**, 32.
- Torres, G. 2007, *ApJ*, **671**, 65.
- von Braun, K., Boyajian, T. S., Kane, S. R., *et al.* 2012, *ApJ*, **753**, 171.